
ACOUSTIC SIGNALS PROCESSING.
COMPUTER SIMULATION

Spatial Correction of an Acoustic Hologram for Reconstructing Surface Vibrations of an Axially Symmetric Ultrasound Transducer

A. Z. Kaloev^a, D. A. Nikolaev^a, V. A. Khokhlova^{a, *}, S. A. Tsysar^a, and O. A. Sapozhnikov^a

^a Lomonosov Moscow State University, Moscow, 119991 Russia

*e-mail: vera@acs366.phys.msu.ru

Received July 18, 2021; revised July 18, 2021; accepted September 22, 2021

Abstract—A method is proposed for spatially correcting an acoustic hologram recorded on an arbitrarily oriented planar area in front of an axially symmetric ultrasound transducer. The method comprises steps for determining the direction of the transducer's axis from the measured acoustic hologram, transferring the hologram data on a plane perpendicular to this axis and centering it relative to the axis by means of a correction algorithm that executes appropriate rotations and shifts of the original hologram. The corrected hologram is used for reconstructing the structure of vibrations of the emitting surface of the transducer. A simplified correction algorithm is also considered that is applicable for transducers with narrow angular spectrum and small angles of inclination of the initial hologram to the transducer axis. The accuracy of the developed algorithms is analyzed numerically for a single focusing transducer with a uniform vibrational velocity distribution on its surface and is demonstrated experimentally for an annular 12-element array.

Keywords: acoustic holography, characterization of ultrasound transducers, therapeutic multi-element arrays

DOI: 10.1134/S1063771022010043

INTRODUCTION

The development of noninvasive therapeutic methods using high-intensity focused ultrasound (HIFU) requires the development of specific standards for the devices used and the fields they generate. Manufacturers of ultrasound transducers typically provide information on the geometric dimensions of a source, its focal length, operating frequency, and the efficiency of electro–acoustic power conversion. However, the real spatial structure of vibrations of the emitting surface is unknown in this case. The nominal geometric parameters of the transducer specified by the manufacturer can be used to calculate the ultrasound field created by the transducer in the approximation of a uniform amplitude distribution of the normal component of the vibrational velocity on its emitting surface. Such an approximation is not always valid, and therefore the acoustic field calculated with this approach may significantly differ from the real one, which is a critical disadvantage for the laboratory and clinical use of ultrasound systems.

To accurately predict the spatio-temporal structure of the ultrasound field, one should proceed from the experimentally reconstructed distribution of the normal component of the vibrational velocity on the surface of the transducer. Such a distribution can be obtained by acoustic holography measurements, which then are used to reconstruct the structure of the acoustic field in the entire space based on a holo-

gram—the measured two-dimensional transverse distribution of the field parameters on a surface in front of the transducer [1–3]. This method has been recently recommended as a standard for characterizing ultrasound transducers [4].

When recording an acoustic hologram, it is necessary to monitor a large number of experimental parameters, which can introduce a systematic error into the structure of the field calculated from the measured hologram [5]. A hologram is usually measured by a miniature receiver in a large number of points of a planar area, the size of which is chosen slightly larger than the diameter of the ultrasound beam in order to ensure complete recording of the acoustic field. In the case of an axially symmetric transducer, the area in which the hologram is measured is conveniently located opposite the transducer, so that the center of the hologram lies on the transducer axis and the normal to the area is directed along this axis. In reality, such ideal positioning of the hologram cannot be ensured: shifts and small angles between the transducer axis and normal to the hologram plane are inevitable [6].

It should be noted that the acoustic hologram contains complete information about the field structure not only for an ideal, but also for an inclined or displaced position of the measurement plane. In this sense, the exact orientation of the recording area of the hologram is not essential—it is only important that the

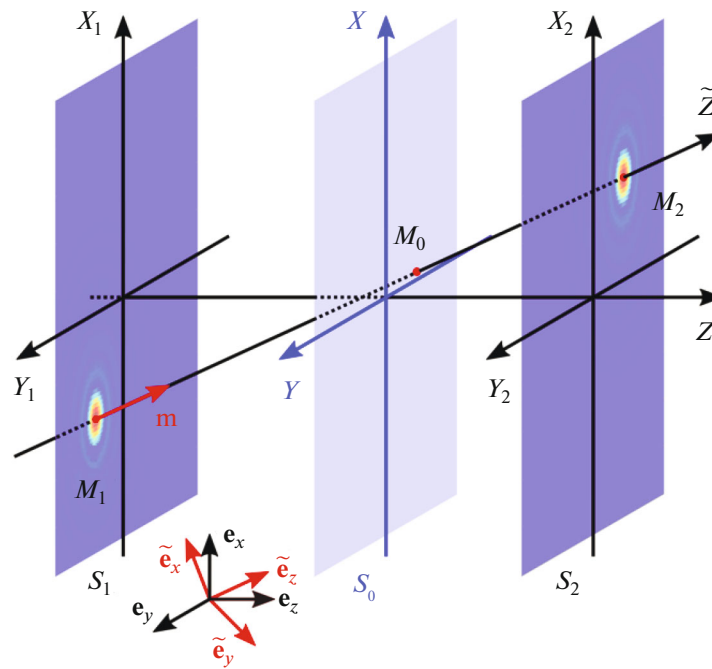


Fig. 1. Diagram of reconstructing the acoustic axis \tilde{Z} of a transducer.

specified area is intersected by the entire ultrasound beam generated by a transducer. However, when analyzing the field and, in particular, when determining the structure of vibrations of the emitting surface, it is more convenient to bring the measured hologram to the coordinates of the transducer by recalculating it to a plane centered on and perpendicular to its axis.

In this paper, we propose a method for such spatial correction of a hologram. We also compare the results of exact correction performed using transformation of the angular spectrum of the hologram with the results of an approximate correction performed by rotating the phase front of the hologram in the ray approximation. The accuracy of the proposed methods is analyzed in a numerical experiment with a single focusing transducer in the form of a uniformly vibrating segment of a spherical surface. Experimental testing of the proposed approaches is also done when reconstructing the structure of vibrations of the surface of an annular 12-element phased array.

SELECTING THE COORDINATE SYSTEMS FOR RECORDING A HOLOGRAM

Consider the acoustic field generated by an axially symmetric source. As a consequence, the field itself is also axially symmetric. The axis of symmetry will be named here as the “acoustic” axis. We will also name as an “ideal” hologram the one that is recorded in a planar area, the center of which is located on the acoustic axis of the transducer and the normal is oriented parallel to this axis. The only parameter deter-

mining the relative position of the ideal hologram and the source is the distance between them; therefore, if it is known, then it is possible to calculate the structure of the transducer’s vibrations. For an arbitrary position of the measured hologram, corresponding calculations are also possible, but they are more difficult, since in this case it is necessary to know several parameters that specify the relative position of the transducer and the hologram. Accordingly, the problem of calculating the vibrational velocity on an emitting surface becomes both theoretically and numerically challenging. An experimentally measured hologram that is generally differs from an ideal one by some shift and rotation will be named as “real.”

Since both the real and ideal holograms are complete recordings of the same wave field, they can be recalculated to each other if their relative orientation in space is known. In practice, an acoustic hologram is measured by scanning the acoustic field with a triaxial micropositioning system. In this case, to set the orientation of the real and ideal holograms, one can naturally use the Cartesian coordinate system, the axes of which are co-directional along three directions of movement in the micropositioning system. We name the indicated X , Y , Z axes as the “mechanical” axes and assume that the measured hologram is the result of scanning the field in the (X, Y) plane (Fig. 1).

The first step in solving the problem of constructing an ideal hologram is to find the acoustic axis of the transducer in the mechanical coordinate system. Let S_0 be a planar area in the (X, Y) plane, in which the initial hologram, i.e., the two-dimensional distribution

of the amplitude and phase or, equivalently, the complex wave amplitude, is recorded. Since the investigated field is axially symmetric, the wave amplitude distribution in the measurement plane (X, Y) of the hologram will also possess a symmetry with a highlighted center even if the recording area is tilted relative to the acoustic axis. When measuring a hologram, we place the origin of the mechanical coordinate system (X, Y, Z) = (0, 0, 0) near this center. The accuracy of coincidence of the center of symmetry of the beam with the origin will be determined by the scanning step; however, exact coincidence at this stage is not essential. When measuring a hologram close to ideal and choosing such an origin, the Z axis will be close to the acoustic axis. Based on the measured hologram, the wave amplitude distribution on the Z axis is calculated by the Rayleigh integral [7] or the angular spectrum method [8–10]. Due to the proximity of the Z axis to the acoustic axis, the obtained distribution will approximately coincide with the pressure distribution along the acoustic axis and contain diffraction maxima and minima.

Next, the auxiliary transverse pressure distributions are calculated in two planar areas S_1 and S_2 , parallel to the plane of the initial hologram and located at distances $z = z_1$ and $z = z_2$, in which the wave amplitude has local maxima (Fig. 1). Similar to finding the field on the Z axis, the field in areas S_1 and S_2 can be calculated by the Rayleigh integral or angular spectrum method. The problem here is to determine as accurately as possible the coordinates of the points where the areas S_1 and S_2 are intersected by the acoustic axis. To speed up calculations, it is convenient to firstly obtain the transverse field distributions at the nodes of a grid with a large step, then approximately find the center of symmetry of the distribution and perform the calculations again in its vicinity with a smaller grid step. As a result, in the areas S_1 and S_2 of the auxiliary planes, we can determine with high accuracy the coordinates $\mathbf{r}_1 = (x_1, y_1, z_1)$ and $\mathbf{r}_2 = (x_2, y_2, z_2)$ of the field maxima M_1 and M_2 , through which the acoustic axis passes.

From the found coordinates of points M_1 and M_2 , we then calculate the coordinates \mathbf{r}_0 of the point M_0 where the acoustic axis of the transducer intersects the plane of the initial hologram, as well as the coordinates of the directing unit vector \mathbf{m} of the acoustic axis:

$$\mathbf{r}_0 = \mathbf{r}_1 - (\mathbf{r}_2 - \mathbf{r}_1) \frac{z_1 - z_0}{z_2 - z_1}, \quad (1)$$

$$\mathbf{m} = \frac{\mathbf{r}_2 - \mathbf{r}_1}{|\mathbf{r}_2 - \mathbf{r}_1|}. \quad (2)$$

Here, $\mathbf{r}_0 = (x_0, y_0, z_0)$ is the radius vector of the point M_0 ; $z_0 = 0$ due to the initial choice of the origin. Vectors \mathbf{r}_0 and \mathbf{m} completely define the acoustic

axis of the transducer. The maximum errors $\Delta \mathbf{r}_0$ and $\Delta \mathbf{m}$ in determining the coordinates of vectors \mathbf{r}_0 and \mathbf{m} are defined by the choice of the grid steps Δx and Δy in the auxiliary holograms and the distances h between them: $\Delta \mathbf{r}_0 = (\Delta x/2, \Delta y/2, 0)$ and $\Delta \mathbf{m} = \frac{1}{h} (\Delta x, \Delta y, \sqrt{(m_x^2 \Delta x^2 + m_y^2 \Delta y^2) / m_z^2})$.

The procedure described above was performed in a mechanical Cartesian coordinate system that corresponds to the three directions of movement in the triaxial micropositioning system. To reconstruct the ideal hologram, we now consider a new Cartesian coordinate system ($\tilde{X}, \tilde{Y}, \tilde{Z}$), the origin of which lies at the point M_0 and the axis \tilde{Z} coincides with the acoustic axis of the transducer. Axes \tilde{X} and \tilde{Y} lie in the plane perpendicular to the transducer axis; therefore, their directions cannot be uniquely defined due to the axial symmetry of the problem. However, it is reasonable to choose them close to the directions of the corresponding X and Y axes. For convenience of describing the two systems, we introduce the unit vectors $\mathbf{e}_x, \mathbf{e}_y, \mathbf{e}_z$ of the initial (mechanical) coordinate system and unit vectors $\tilde{\mathbf{e}}_x, \tilde{\mathbf{e}}_y, \tilde{\mathbf{e}}_z$ of the new system, “attached” to the transducer (Fig. 1). According to this definition:

$$\tilde{\mathbf{e}}_z = \mathbf{m} = (m_x, m_y, m_z). \quad (3)$$

The unit vectors $\tilde{\mathbf{e}}_x$ and $\tilde{\mathbf{e}}_y$ in the old basis can be introduced, e.g., as

$$\begin{aligned} \tilde{\mathbf{e}}_y &= \frac{\tilde{\mathbf{e}}_z \times \mathbf{e}_x}{|\tilde{\mathbf{e}}_z \times \mathbf{e}_x|} = \left(0, \frac{m_z}{\sqrt{m_z^2 + m_y^2}}, -\frac{m_y}{\sqrt{m_z^2 + m_y^2}} \right), \quad (4) \\ \tilde{\mathbf{e}}_x &= \tilde{\mathbf{e}}_y \times \tilde{\mathbf{e}}_z \\ &= \left(\sqrt{m_z^2 + m_y^2}, -\frac{m_x m_y}{\sqrt{m_z^2 + m_y^2}}, -\frac{m_x m_z}{\sqrt{m_z^2 + m_y^2}} \right), \quad (5) \end{aligned}$$

where the sign \times denotes vector multiplication.

Note that the new basis chosen in this way can be obtained from the old one by two successive rotations: first around the X axis by an angle α , then around the new axis \tilde{Y} obtained after the first rotation by an angle β , which are determined by the following expressions:

$$\alpha = -\arcsin(\tilde{\mathbf{e}}_y \mathbf{e}_z) = \arcsin\left(\frac{m_y}{\sqrt{m_z^2 + m_y^2}}\right), \quad (6)$$

$$\beta = -\arcsin(\mathbf{e}_x \tilde{\mathbf{e}}_z) = -\arcsin(m_x), \quad (7)$$

where scalar multiplication of the vectors is applied. The first rotation makes the \tilde{Y} axis perpendicular to the vector \mathbf{m} , and the second one makes the \tilde{X} axis perpendicular to the vectors \mathbf{m} and $\tilde{\mathbf{e}}_y$. Hereinafter, the positive angle of rotation of a hologram or coordinate system around any axis corresponds to a clockwise

rotation in the right coordinate system, if viewed in the direction opposite to the axis around which the rotation occurs.

CALCULATING THE IDEAL HOLOGRAM FROM THE REAL ONE

At the second stage of constructing the ideal hologram, the relationship between the two coordinate systems described above is used. It is convenient to transfer the hologram from one system to another using the angular spectrum method. The spatial (angular) spectrum $S(k_x, k_y)$ of the field in the plane of the measured hologram $p_0(x, y)$ has the form [8]

$$S(k_x, k_y) = \int_{-\infty}^{+\infty} \int_{-\infty}^{+\infty} p_0(x, y) e^{-i(k_x x + k_y y)} dx dy. \quad (8)$$

For a known spectrum $S(k_x, k_y)$, the complex pressure amplitude $p(x, y, z)$, which is the solution to the Helmholtz equation, is expressed as follows:

$$p(x, y, z) = \frac{1}{(2\pi)^2} \times \iint_{k_x^2 + k_y^2 \leq k^2} S(k_x, k_y) e^{i(k_x x + k_y y + \sqrt{k^2 - k_x^2 - k_y^2} z)} dk_x dk_y, \quad (9)$$

where $k = \omega/c$ is the wavenumber, ω is the angular frequency of the wave, and c is the sound speed.

Here, the integration domain is limited to a circle of radius k , which is valid at distances from the transducer much longer than the wavelength. Strictly speaking, to write the exact solution (9), the integration domain should be extended to the entire plane, which makes it possible to take into account inhomogeneous (evanescent) waves [1]. However, these inhomogeneous waves decay rapidly with the distance from the transducer, and therefore, for ultrasound in the megahertz range used in medicine and nondestructive testing, their influence can be neglected. The wave field representation (9) has the form of the superposition of plane waves with a complex amplitude proportional to the quantity $S(k_x, k_y) \exp(i \mathbf{k} \mathbf{r})$, and the wave vector \mathbf{k} in the (X, Y, Z) coordinate system has the form:

$$\mathbf{k} = \left(k_x, k_y, k_z = \sqrt{k^2 - k_x^2 - k_y^2} \right). \quad (10)$$

We now consider the new coordinate system $(\tilde{X}, \tilde{Y}, \tilde{Z})$ centered at the point M_0 . The radius vector of the point in space is expressed as follows: $\mathbf{r} = \tilde{x} \tilde{\mathbf{e}}_x + \tilde{y} \tilde{\mathbf{e}}_y + \tilde{z} \tilde{\mathbf{e}}_z + \mathbf{r}_0$. In the new coordinate system, expression (9) is transformed to

$$P(\tilde{x}, \tilde{y}, \tilde{z}) = \frac{1}{(2\pi)^2} \times \iint_{k_x^2 + k_y^2 \leq k^2} S(k_x, k_y) e^{i[\tilde{x}(\mathbf{k}\tilde{\mathbf{e}}_x) + \tilde{y}(\mathbf{k}\tilde{\mathbf{e}}_y) + \tilde{z}(\mathbf{k}\tilde{\mathbf{e}}_z) + (\mathbf{k}\mathbf{r}_0)]} dk_x dk_y, \quad (11)$$

where $P(\tilde{x}, \tilde{y}, \tilde{z}) = p(x, y, z)$ is the complex wave amplitude recorded in the new coordinates. The scalar products in the exponent are easily calculated using the relations (3)–(5).

Let us choose the plane $\tilde{z} = 0$ passing through the point M_0 as the plane for setting the ideal hologram $P_0(\tilde{x}, \tilde{y})$. For this choice, $P_0(\tilde{x}, \tilde{y}) = P(\tilde{x}, \tilde{y}, \tilde{z} = 0)$, and therefore, the representation for the ideal hologram follows from the expression (11):

$$P_0(\tilde{x}, \tilde{y}) = \frac{1}{(2\pi)^2} \times \iint_{k_x^2 + k_y^2 \leq k^2} S(k_x, k_y) e^{i[\tilde{x}(\mathbf{k}\tilde{\mathbf{e}}_x) + \tilde{y}(\mathbf{k}\tilde{\mathbf{e}}_y) + (\mathbf{k}\mathbf{r}_0)]} dk_x dk_y, \quad (12)$$

where the terms in the exponent are given by the expressions (1)–(5) and (10). Note that in the case of a small angle between the normal to the initial hologram and the acoustic axis of the transducer, as well as the narrowness of the angular spectrum of the beam, expression (12) is simplified:

$$P_0(\tilde{x}, \tilde{y}) \approx e^{-ik(m_x \tilde{x} + m_y \tilde{y})} p_0(\tilde{x} + x_0, \tilde{y} + y_0). \quad (13)$$

Clearly, in the indicated approximation, the transition (13) from the measured $p_0(x, y)$ to the ideal hologram $P_0(\tilde{x}, \tilde{y})$ corresponds to displacement of the center of the coordinates of the initial hologram to the point M_0 and multiplication by an additional phase incursion, which increases along the transverse coordinates, as for a plane wave propagating in the direction of the vector \mathbf{m} . As noted, the first condition for the validity of the approximation (13) is the requirement that the angles of rotation are small, which corresponds to the condition $\sqrt{m_x^2 + m_y^2} \ll 1$. In practice, this is relatively easy to perform, since with proper care, transducers with a diameter of several centimeters can even manually be oriented relative to the axes of the positioning system with an error not exceeding 1° or 2° . The second condition is the localization of the angular spectrum in a narrow frequency range $\sqrt{k_x^2 + k_y^2} \ll k$, which depends on the transducer parameters. For example, when using surgical HIFU transducers, the angular spectrum of the wave can be quite broad and, therefore, expression (13) for rotating and centering the hologram will be less precise.

It should be noted that the fast Fourier transform (FFT) algorithm cannot be used to accurately rotate and center the measured hologram, since when the integral in the equation (12) is reduced to the inverse

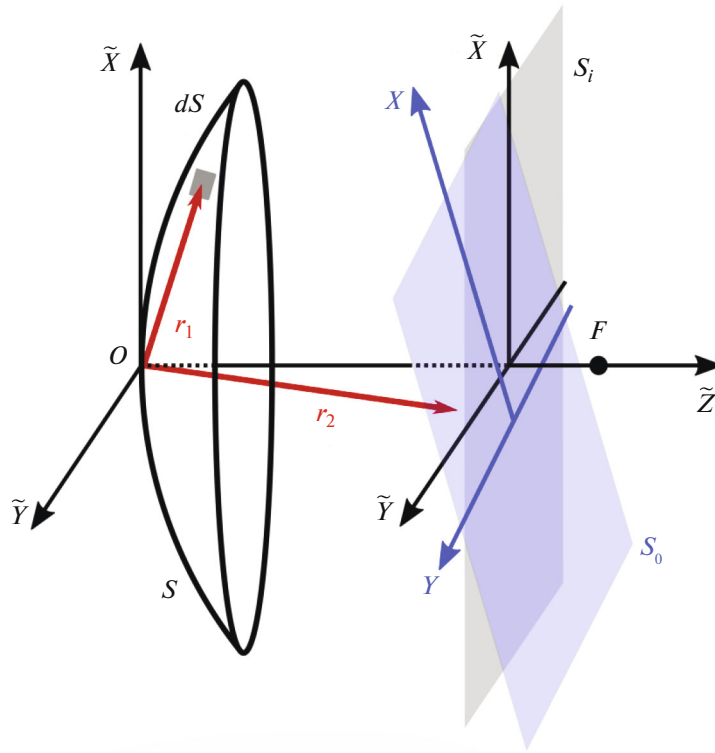


Fig. 2. Diagram of a single transducer in the form of a spherical segment relative to a planar surface of the initial hologram S_0 and the surface of an ideal hologram S_i .

Fourier transform, i.e., when factorizing the integrand as $S_1(k_x, k_y, \mathbf{r}) \exp(i\mathbf{kr})$, the equivalent spectrum $S_1(k_x, k_y, \mathbf{r})$ will depend on the coordinates of the vector \mathbf{r} . Thus, to accurately correct the hologram, it is necessary either to numerically calculate the integral (12) or to implement discrete Fourier transform (DFT) with a spectrum depending on the coordinates. In this study, we used the second method in the calculations; the spectrum $S(k_x, k_y)$ of the initial hologram was computed using FFT. Due to the large number of points in the hologram, its exact correction can take considerable time, especially for large holograms, while approximate rotation and centering according to the equation (13) can be done very quickly by multiplying the hologram by the corresponding exponential matrix. Therefore, it is of interest to study both correction methods, as well as to analyze the error introduced when using the approximate equation (13).

NUMERICAL VERIFICATION OF THE METHOD

We carried out a numerical experiment to analyze the proposed algorithm for obtaining an ideal hologram and reconstructing the distribution of the normal component of the vibrational velocity on the emitting surface; as an example, we used a single-element spherical transducer with an operating frequency

of $f_0 = 2$ MHz, radius of curvature of $F = 80$ mm, and diameter of $D = 100$ mm (Fig. 2). The selected frequency, shape, and dimensions of the transducer corresponded to the parameters of the annular phased array described in the next experimental section.

On the surface S of the transducer, a uniform vibrational velocity distribution of unit amplitude was set, and the pressure on the surface S_0 of the non-ideal hologram was calculated using the Rayleigh integral:

$$P(\mathbf{r}_2) = -\frac{ik\rho c}{2\pi} \int_S V_n(\mathbf{r}_1) \frac{e^{ikR}}{R} dS, \quad (14)$$

where $R = |\mathbf{r}_1 - \mathbf{r}_2|$, \mathbf{r}_1 is the radius vector of the surface element dS and \mathbf{r}_2 is the radius vector of the point at which the complex pressure amplitude P is calculated. The angle between the normal to the hologram surface and the axis of the transducer $O\tilde{Z}$ was chosen nonzero, and the center of the site S_0 was displaced relative to the axis of the transducer (Fig. 2).

To calculate a non-ideal hologram S_0 according to the equation (14), it is necessary to know the equation of the plane of the given hologram. It was derived from the equation of the plane in which the ideal hologram S_i lies by its two successive rotations: the first one around the axis \tilde{Y} , and then around the new axis X obtained after the first rotation; as well as by the dis-

placement of the center of coordinates in the plane of the rotated hologram. Thus, to unambiguously set the position of the plane of the real hologram, five parameters were used: the distance from the center of the source O to the center of the ideal hologram S_i , the angles of its rotations around the axes \tilde{Y} and the new axis X , as well as the displacement of the center of the hologram along the axes X and Y (Fig. 2).

After calculating the pressure distribution on the surface S_0 (Fig. 2) by (14), the described algorithm for finding the acoustic axis of the transducer was applied, then the hologram was rotated and centered using the exact (12) and the approximate (13) methods. Two new calculated holograms and the initial non-ideal hologram were used in Rayleigh integral calculations to reconstruct the amplitude and phase distributions of the normal component of the vibrational velocity on a surface of a spherical segment cut off by the used hologram from a sphere of $F = 80$ mm radius centered on the assumed acoustic axis and located at some distance from the hologram. In the case of correction, it was assumed that the acoustic axis passed perpendicular to the plane of the corrected hologram through its center M_0 (1), and in the absence of correction, perpendicular to the plane of the initial hologram through the grid node closest to the field's center of symmetry. The distance from the holograms to the spherical surface was obtained by superposing the maxima of the pressure amplitude distributions on the axis calculated using the Rayleigh integral (14) for the nominal parameters of the transducer and reconstructed from the used holograms. Beyond the surface of the spherical segment cut off by the hologram, the amplitude and phase of the vibrational velocity were assumed to be zero.

The plane of the non-ideal hologram S_0 was obtained from the plane of the ideal hologram S_i at a distance of 70 mm from the center O of the transducer (Fig. 2). The size of the hologram was chosen as 301×301 points with a step of $dx = dy = 0.35$ mm, which corresponded to 0.47 of the ultrasound wavelength in water at the operating frequency of the transducer. The final grid step on the auxiliary planes (Fig. 1) was 0.01 mm, which corresponded to the maximum error of 0.014 mm in determining the coordinates of the center of symmetry in the obtained non-ideal holograms.

Three cases of deviation of the initial hologram from the ideal one were considered. In the first case, an imperfect hologram was obtained by rotating and displacing the ideal hologram by relatively large values compared to the characteristic experimental values: the angles of rotation around the \tilde{Y} and X axes were 4° and -4° , respectively, and the center of the hologram was displaced to the point $(x_0, y_0) = (2, 4)$ mm. In the second case, small angles of rotation and displacement of the ideal hologram were considered: the angles of rotation around the \tilde{Y} and X axes were 1° and -1° ,

respectively, and the center of the hologram was displaced to the point $(x_0, y_0) = (1, 1)$ mm. In the third case, to quantitatively estimate the accuracy of reconstructing the vibrational velocity on the surface of the transducer using the exact and approximate correction methods, we calculated the holograms that were not displaced relative to the ideal one, but were rotated around the \tilde{X} axis by a varying angle $0^\circ \leq \alpha \leq 20^\circ$. In this case, the hologram was set on a grid consisting of 201×201 points.

For the first case of large rotation and displacement of the plane of the ideal hologram, Fig. 3 shows the results of calculating the pressure amplitude and phase in the central part of the obtained non-ideal hologram, as well as after its approximate and exact corrections. In the absence of correction (Fig. 3a), the displacement of the center of the hologram and violation of the symmetry of the distributions for both the amplitude and the pressure phase are distinctly notable. After the approximate correction (Fig. 3b), both the pressure amplitude and phase distributions become centered. The angular asymmetry in the phase distribution over the angle around the beam axis decreases significantly, but remains unchanged in the amplitude distribution, since the approximate correction (13) represents a shift of the center of the coordinate system and multiplication by the phase factor. After the exact correction (Fig. 3c), both the amplitude and phase become symmetrical about the center of the hologram. Inverse displacement of the center of the hologram and angles of rotation during the correction calculated from (1), (6), (7) are $(-2.00, -3.99)$ mm and $(-3.99, 3.97)^\circ$.

Figure 4 shows the initially set amplitude and phase distributions of the normal component of the vibrational velocity on the surface of the transducer (Fig. 4a) and those reconstructed from the obtained holograms (Fig. 3). When reconstructing without correction, the hologram is centered by shifting the center of coordinates to the grid node with coordinates $(-2.10, -3.85)$ mm, which is the closest node to the center of symmetry of the hologram field. Clearly (Fig. 4b), the greater inaccuracy in finding the coordinates of the center did not induce a noticeable effect on the uniformity of the reconstructed pressure amplitude distribution on the surface of the sphere, but the expected displacement of the transducer surface did occur along the spherical surface on which the calculation was carried out. In the case of the approximate correction of the hologram (Fig. 4c), the amplitude distribution is different from the initial one (Fig. 4a) both in nonuniformity along the surface and in the non-sharp boundary of the transducer. In this case, the observed differences are even stronger than without correction of the hologram, which illustrates the inaccuracy of the approach. The phase distribution became more uniform, but still differs from the initial one. With exact correction of the hologram, the calcu-

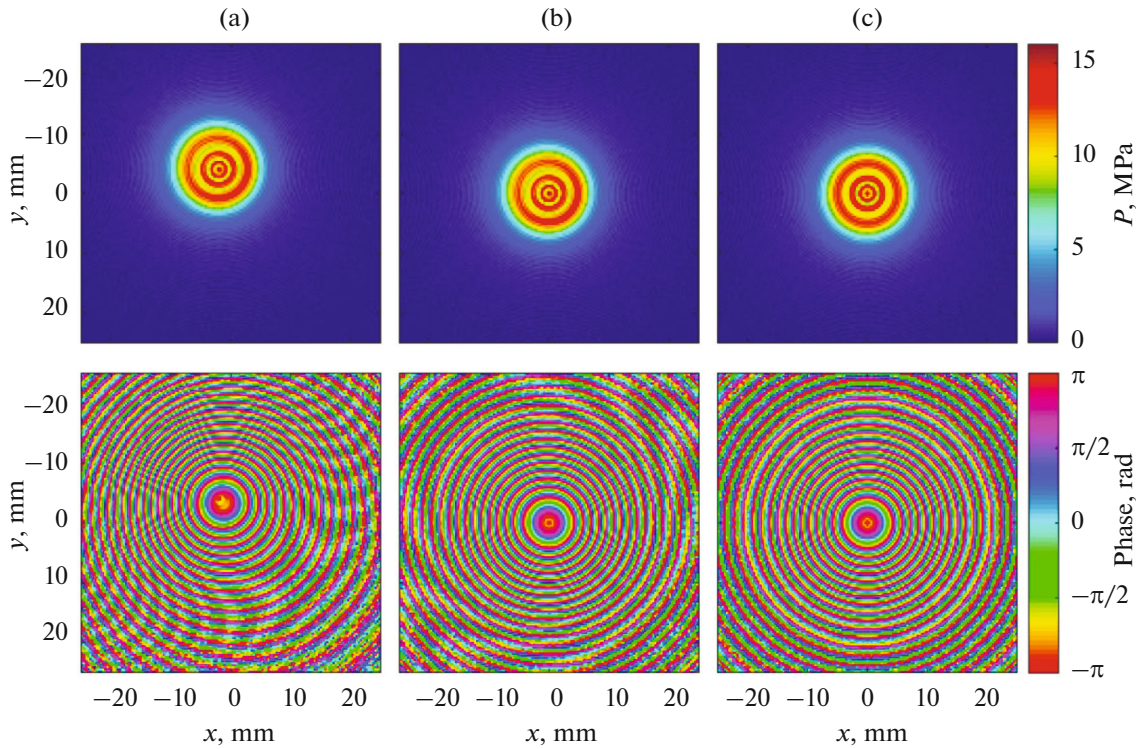


Fig. 3. Distribution of amplitude (top) and phase (bottom) in the plane of: (a) initial hologram S_0 with large rotation and displacement of its plane relative to the ideal hologram, (b) hologram corrected by the approximate method, (c) hologram corrected by the exact method.

lated structure of the transducer vibrations practically coincides with the initial one (Fig. 4d). There is only a slight inhomogeneity in the amplitude distribution at the edges of the transducer, which occurs due to the neglect of inhomogeneous waves when the angular spectrum method is used to calculate the solution (9). In real measurements, the hologram recording errors can also introduce an additional error in the given quantities [5].

For clarity, Fig. 5 compares the obtained amplitude (Fig. 5a) and phase (Fig. 5b) distributions on the surface of the transducer along the X axis for $y = 0$. The red curve corresponds to the distribution obtained after exact correction of the hologram. As can be seen, it is very close to the initially specified rectangular distribution (gray curve), whereas the results obtained with approximate correction or without correction (black and blue curves, respectively) differ greatly from the true ones.

For the second case of small rotation angles and displacement of the initial hologram relative to the ideal one, the results of reconstructing the amplitude and phase of the vibrational velocity on the transducer surface are shown in Fig. 6. The corrected inverse displacement of the center of the hologram and rotation angles were $(-1.01, -1.01)$ mm and $(-1.01, 1.01)^\circ$ as compared to the initially specified ones $(1.00, 1.00)$ mm

and $(1.00, -1.00)^\circ$; when reconstructing without correction, the center of the coordinate was shifted to the grid point with coordinates $(-1.05, -1.05)$ mm. On the whole, in the reconstructed distributions, although to a less extent, the same differences are observed as in the case of large angles and displacements. It is worth noting that although in this case application of the approximate method is more justified, both the amplitude and phase distributions of the vibrational velocity at the transducer (Fig. 6c), obtained from the approximately corrected hologram, still differ from the initial ones (Fig. 6a). This is because the angular spectrum of the field of the considered HIFU transducer is quite broad.

For the third case of different rotation angles α of the hologram relative to the ideal one and use of the exact and approximate correction methods, the magnitude of the error in determining the vibrational velocity on the surface of the transducer was estimated quantitatively. From the obtained holograms, the vibrational velocity on the assumed surface of the transducer was calculated without correction and after approximate and exact rotation of the hologram. As mentioned above, due to the neglect of inhomogeneous waves [8] even calculating an ideal hologram from the boundary condition set on the transducer surface and making the inverse calculation, the obtained distribution of the vibrational velocity on the

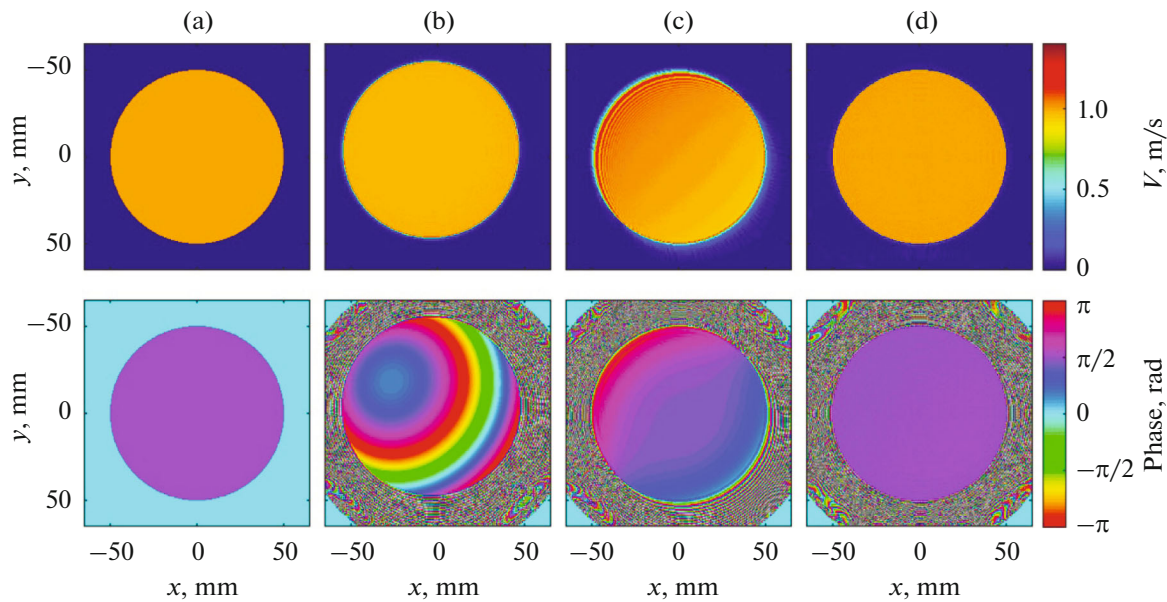


Fig. 4. Distribution of amplitude (top) and phase (bottom) of normal component of vibrational velocity at the transducer's surface: (a) initially specified; calculated from (b) the initial hologram in case of large rotation and displacement of its plane relative to the ideal hologram, (c) approximately corrected hologram, (d) exactly corrected hologram.

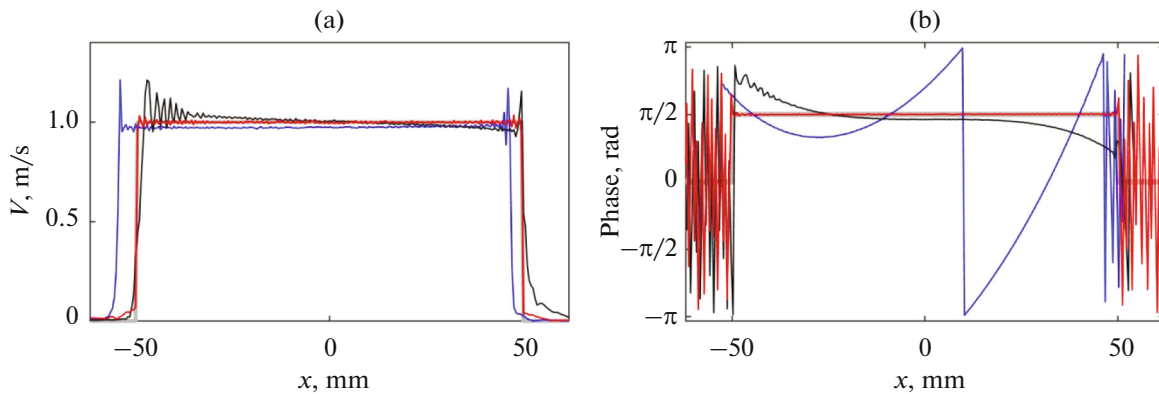


Fig. 5. (a) Amplitude and (b) phase of normal component of surface's vibrational velocity along the axis X for $y = 0$. Gray line corresponds to the initially specified rectangular distribution; blue curve corresponds to that reconstructed from the initial hologram without correction for large rotation angles and displacement of its plane relative to the ideal hologram; red and black lines correspond to those reconstructed from the holograms corrected by the exact and approximate methods, respectively.

transducer will not be identical to the initial one. Therefore, the error $\varepsilon(\alpha)$ in the vibrational velocity distribution calculated at the transducer $V_n(\alpha)$ arising after the exact and approximate rotations was considered with respect to the numerically reconstructed distribution $V_n(\alpha = 0)$:

$$\varepsilon(\alpha) = \frac{1}{N} \sum_n^N |V_n(\alpha) - V_n(\alpha = 0)|, \quad (15)$$

where N is the number of grid points on the surface of the spherical segment cut off by a hologram from a

sphere of radius $F = 80$ mm, on which the velocity distribution is reconstructed.

Figure 7 compares the error introduced in this way for the three described cases. As expected, as the angle between the normal to the hologram and the transducer axis increases, the error in determining the vibrational velocity on the transducer surface that occurs after the approximate correction of the hologram increases much faster than in the case of the exact correction. The appearance of a small error when using the exact correction method is associated both with some inaccuracy in determining the direction of the acoustic axis and, correspondingly, the

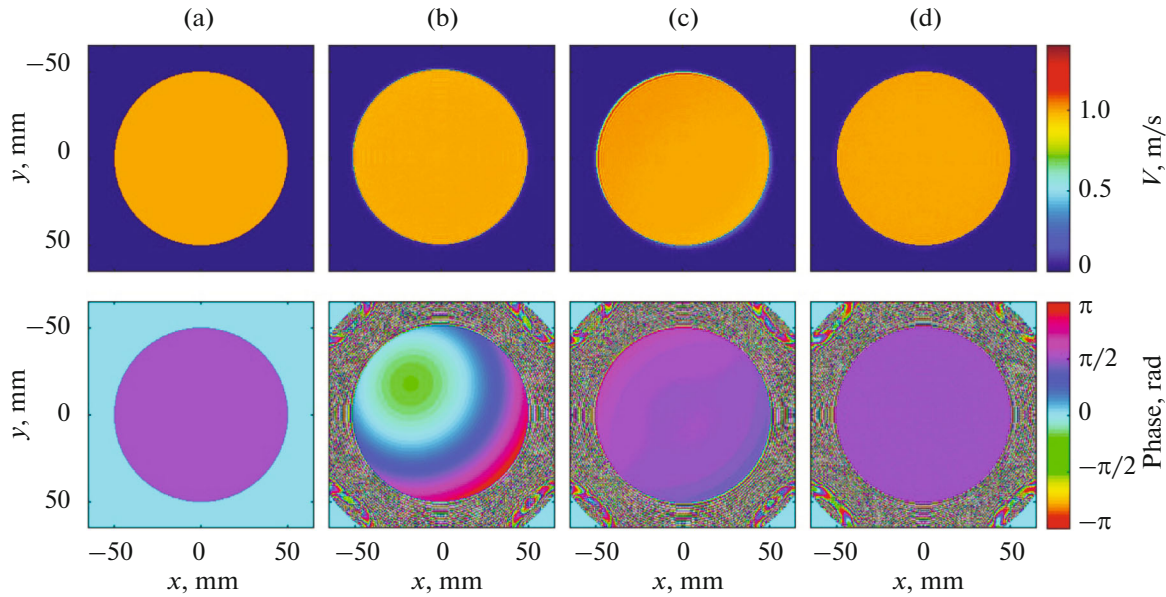


Fig. 6. Distribution of amplitude (top) and phase (bottom) of normal component of vibrational velocity at the transducer's surface: (a) initially specified; calculated from (b) the initial hologram for small rotation angles and displacement of its plane relative to the ideal hologram, (c) approximately corrected hologram, (d) exactly corrected hologram.

coordinates of vectors \mathbf{m} and \mathbf{r}_0 (1), (2), and with the fact that for higher angles of rotation, due to the fixed size of the hologram, less beam energy is incident on its surface, so it contains less complete information about the acoustic field.

EXPERIMENTAL VERIFICATION OF THE METHOD

The method was verified experimentally for a piezocomposite annular focusing transducer (Imasonic, France) (Fig. 8) in the shape of a concave spherical bowl with a circular central hole. The transducer has the following parameters: inner and outer diameters $D_1 = 40$ mm and $D_2 = 100$ mm, respectively; focal length (radius of curvature) $F = 80$ mm; resonance frequency $f_0 = 2$ MHz. The emitting surface of the transducer is divided into 12 annular segments of equal area $S = 5.2$ cm² with a gap of $dr = 0.5$ mm between two neighboring rings, which allows the transducer to be used as an annular phased array.

The transducer was immersed in a $100 \times 50 \times 50$ cm tank with degassed water and fixed in place during measurements. The water was filtered and degassed with a PA WTS (water treatment system, Precision Acoustics, UK). Each element of the phased array was supplied with electric voltage from a 12-channel generator [11]. An HNA-0400 needle hydrophone (Onda Corp., USA) with a sensor area 0.4 mm in diameter was placed opposite the array. The sensitivity of the hydrophone, taking into account the built-in preamplifier of the electrical signal, was 1.197 V/MPa at fre-

quency 2 MHz. During measurements, the hydrophone was moved automatically with the UMS-3 micropositioning system (Precision Acoustics, UK) positioned above the tank, allowing 3D scanning with guaranteed positioning accuracy of 6 μ m. The electrical signal from the hydrophone was fed to an oscilloscope (TDS5054B, Tektronix Inc., USA) connected to a computer. The measurement process was controlled by a program written in the LabView environment, which is part of the Precision Acoustics positioning system. Water temperature stability during measurements was maintained by a thermocouple built into the transducer. The hologram measurement

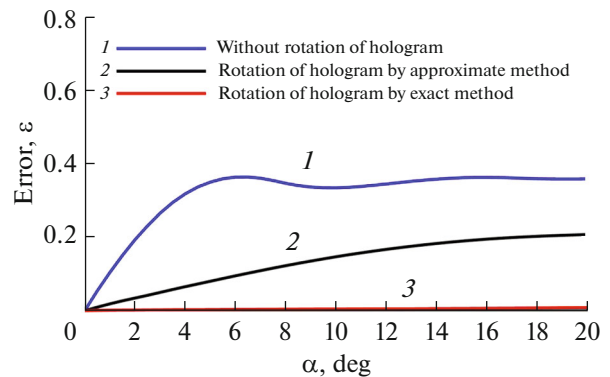


Fig. 7. Dependence of the error in determining a distribution of the complex amplitude of normal component of vibrational velocity on the angle of inclination of a hologram plane to transducer's axis for the exact (red line 3) and approximate (black line 2) hologram correction, as well as without correction (blue line 1).

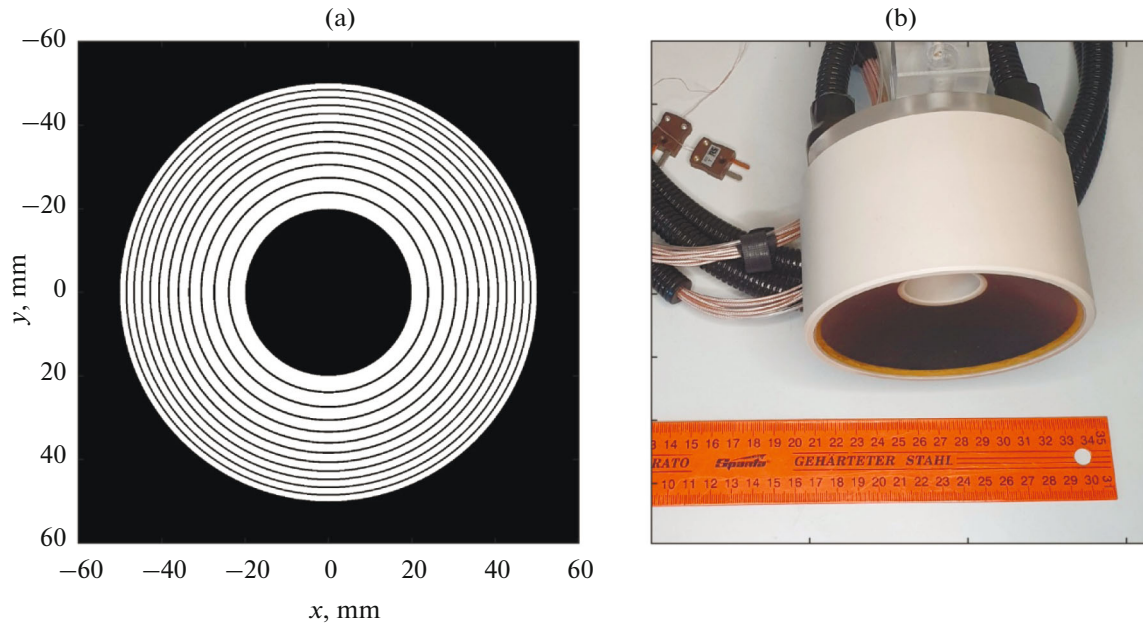


Fig. 8. (a) Diagram and (b) photograph of the ultrasound phased array (Imasonic, France) used in holography measurements. The array comprises 12 rings of equal area, located on the sphere of $F = 80$ mm radius.

time was approximately 10 hours, during which the temperature deviation from 22°C was no more than 0.3°C .

Two holograms were measured: the first one was recorded when the transducer was positioned parallel to the hologram measurement plane with an accuracy of about 1° ; the second one was measured after rotating the transducer by 10° around the Y axis of the hologram. Rotation was done via the rotary mechanism of the positioning system with a nominal angle-setting accuracy up to 0.2° . The hologram was recorded by measuring the hydrophone signal at the nodes of a plane square grid with a step of 0.4 mm, located 15 mm from the focal maximum towards the transducer. The corresponding number of grid nodes was chosen as 221×221 , the size of the hologram in each measurement exceeded the geometric size of the ultrasound beam in this region by a factor of 3.6. The center of the region and scanning in both cases were set manually in the center of the acoustic beam to ensure that the acoustic beam passed through the measurement area to the fullest extent.

All annular elements of the transducer were excited in phase by an electric pulse consisting of $N = 5$ periods at $f_0 = 2$ MHz frequency and 1 V amplitude; the pulse repetition rate was $T = 4$ ms. The signal at each point of the hologram was recorded within a $100 \mu\text{s}$ time window, which was sufficient to record the pulsed acoustic signal by the hydrophone in each point of the hologram. The hydrophone signal was recorded at a sampling rate of 20 ns, which included 5000 time samples for the selected time window. To reduce the noise

level at each point of the hologram, averaging was performed over 48 samplings of the periodically repeating signal. The measurements yielded a nonstationary hologram, from which the hologram at the transducer resonance frequency was extracted using spectral decomposition and then was normalized to the corresponding frequency component of the voltage signal spectrum on the elements. After taking into account the sensitivity of the hydrophone, we obtained the distribution of the complex pressure amplitude (in Pa) in the plane of the measured hologram; it corresponded to operation of the array in the monochromatic mode at the resonance frequency with the voltage of 1 V across the elements.

The data obtained by these methods were used to reconstruct the distribution of vibrations of the transducer surface after preliminary exact and approximate corrections of the measured holograms. The auxiliary pressure distributions in the planar areas S_1 and S_2 (Fig. 1) were calculated at the distances of -15.07 and 14.75 mm from the initial holograms, respectively, and the field in them was calculated iteratively by the Rayleigh integral in a window with 50×50 points; the final grid step was 0.01 mm.

In the first case, for correcting the measured hologram that was located close to the ideal one, it was necessary to move the center of the coordinates to the point $(0.06, 0.27)$ mm and perform rotation around the X axis by -0.15° and then around \tilde{Y} by 0.44° . The distance from the plane of the corrected holograms to the maximum amplitude distribution on the transducer axis was 15.01 mm. The amplitude and phase

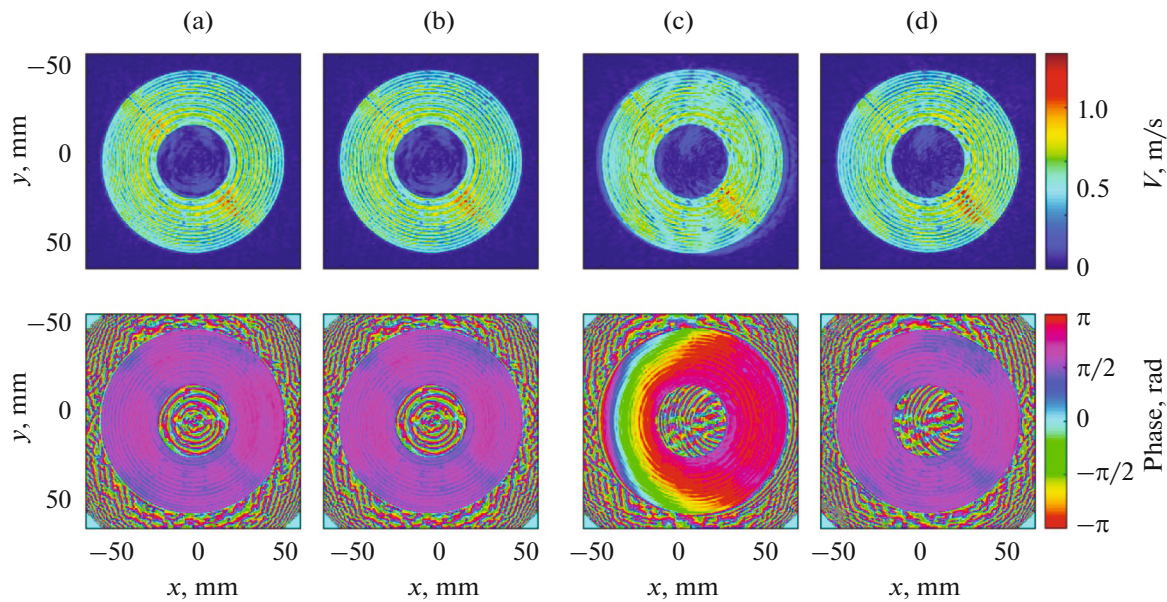


Fig. 9. Comparison of amplitude (top) and phase (bottom) distributions of normal component of vibrational velocity on the surface of a phased array reconstructed from holograms measured at (a, b) small and (c, d) large rotation angles of the hologram plane relative to the acoustic axis of the array after correction (a, c) by the approximate and (b, d) the exact methods.

distributions of the vibrational velocity reconstructed on the assumed surface of the transducer described above turned out to be almost indistinguishable after both approximate (Fig. 9a) and exact (Fig. 9b) corrections.

In the second case, when the transducer axis was rotated with respect to the axes of the positioning system by a sufficiently large angle, to reconstruct the ideal hologram, the center of the coordinates was moved to the point $(-0.08, 0.15)$ mm and the initial hologram was rotated around the X axis by -0.19° and around the \tilde{Y} by -9.57° . The distances from the approximately and exactly corrected holograms to the focus were 13.60 and 15.08 mm, respectively. In this case, the approximate method of correcting the hologram yields unsatisfactory results (Fig. 9c). Note that the distribution of the vibrational velocity on the transducer surface obtained even from the exactly corrected hologram (Fig. 9d) somewhat differs from that calculated at a small rotation angle (Fig. 9b). This discrepancy may be due to the neglect of the hydrophone directivity pattern, which introduces additional distortions when measuring the hologram on a rotated plane [12].

CONCLUSIONS

The paper proposes a method for spatially correcting acoustic holograms of transducers with axial symmetry for practical use in characterizing vibrations of the transducer surface and the fields generated by the transducer. The method allows for constructing a hologram on a plane perpendicular to the transducer axis and centered relative to it, which provides the

most convenient geometry for subsequent setting the boundary conditions on the transducer surface for performing numerical experiments, field reconstruction, and comparison with measurement data in the transducer coordinates. The error of the exact and approximate methods of hologram correction is analyzed at various angles between the axis of the transducer and the normal to the initial hologram. It is shown that, while the approximate correction method is much simpler and faster, its use for sources with a broad angular spectrum may introduce significant errors in reconstruction of an ideal hologram even at small angles of inclination of the hologram plane to the transducer axis. Thus, for medical ultrasound applications requiring high accuracy in determining the structure of vibrations of a transducer surface and the field generated by the transducer, correction of the acoustic hologram using the exact method is preferable.

FUNDING

The study was supported by the grant from the Russian Science Foundation 19-12-00148 and a student summer scholarship from the Focused Ultrasound Foundation.

CONFLICT OF INTEREST

The authors declare that they have no conflicts of interest.

REFERENCES

1. J. D. Maynard, E. G. Williams, and Y. Lee, *J. Acoust. Soc. Am.* **78** (4), 1395 (1985).

2. O. A. Sapozhnikov, Yu. A. Pishchal'nikov, and A. V. Morozov, *Acoust. Phys.* **49** (3), 354 (2003).
3. O. A. Sapozhnikov, A. E. Ponomarev, and M. A. Smagin, *Acoust. Phys.* **52** (3), 324 (2006).
4. *Standard IEC/TS62556: Ultrasonics-Field Characterization-Specification and Measurement of Field Parameters for High Intensity Therapeutic Ultrasound (HITU) Transducers and Systems*, 1st ed. (International Electrotechnical Commission, Geneva, 2014).
5. O. A. Sapozhnikov, S. A. Tsysar, V. A. Khokhlova, and W. Kreider, *J. Acoust. Soc. Am.* **138** (3), 1515 (2015).
6. D. A. Nikolaev, S. A. Tsysar, and O. A. Sapozhnikov, *Bull. Russ. Acad. Sci.: Phys.* **85** (6), 658 (2021).
7. N. T. O'Neil, *J. Acoust. Soc. Am.* **21**, 516 (1949).
8. W. Goodman, *Introduction to Fourier Optics* (McGraw-Hill, New York, 1968).
9. P. R. Stepanishen, *J. Acoust. Soc. Am.* **71**, 803 (1982).
10. M. E. Schafer and P. A. Lewin, *J. Acoust. Soc. Am.* **85** (5), 2202 (1989).
11. A. D. Maxwell, P. V. Yuldashev, W. Kreider, T. D. Khokhlova, G. R. Schade, T. L. Hall, O. A. Sapozhnikov, M. R. Bailey, and V. A. Khokhlova, *IEEE Trans. Ultrason., Ferroelect. Freq. Control* **64** (10), 1542 (2017).
12. M. A. Ghanem, A. D. Maxwell, W. Kreider, B. W. Cunitz, V. A. Khokhlova, O. A. Sapozhnikov, and M. R. Bailey, *IEEE Trans. Ultrason., Ferroelect. Freq. Control* **65** (9), 1618 (2018).